Journal of Organometallic Chemistry xxx (2018) 1–13

Contents lists available at ScienceDirect

Journal of Organometallic Chemistry

journal homepage: www.elsevier.com/locate/jorganchem

Carbon-carbon bonds with CO_2: Insights from computational studies

Marc Obst [1], Ljiljana Pavlovic [1], Kathrin H. Hopmann*

Hylleraas Centre for Quantum Molecular Sciences, Department of Chemistry, University of Tromsø - The Arctic University of Norway, N-9037 Tromsø, Norway

ARTICLE INFO

Article history:
Received 30 November 2017
Received in revised form
13 February 2018
Accepted 14 February 2018
Available online xxx

Keywords:
CO_2
Carboxylic acids
Transition metal
Mechanism
DFT
Computational

ABSTRACT

In this mini-review, we provide an overview of recent computational studies on homogeneous transition metal-catalyzed carbon-carbon bond formation with CO_2. We cover substitution and addition reactions involving different metals (mainly Ni, Rh, Cu) and substrates (alkanes, alkenes, alkynes, arenes) with focus on the mechanistic details. The CO_2 insertion step is generally found to be rate-limiting. The reported transition state geometries for C-C bond formation mostly display three-membered cyclic arrangements involving the metal and the two reacting carbon atoms, except for reaction with C_{sp} atoms, where acyclic conformations are observed. Other reported exceptions point to that an interaction of CO_2 with the metal catalyst may not be essential. Several studies suggest that Lewis acid additives could help activating CO_2 during C-C bond formation.

1. Introduction

CO_2 can be used as a reagent in the synthesis of a variety of chemical building blocks including carbonates, carbamates, carboxylic acids and derivatives (for relevant reviews see Refs. [1–18]). For formation of these molecules, two metal-catalyzed strategies have found widespread use, respectively leading to the formation of C-CO_2 and O/N-CO_2 bonds (Fig. 1).

Rational improvement of CO_2–converting catalysts requires insights into their mechanistic details. Computational studies are often used to understand the activation, selectivity and reaction pathways of homogeneous catalysts. For reactions involving CO_2, relevant computational studies were reviewed in 2012 by both Lin and co-workers [19] and Kühn and co-workers [20]. Both reviews were thematically broad, covering examples of reduction of CO_2 to CO, hydrogenation of CO_2 to formate, reaction of CO_2 with epoxides or alcohols to form carbonates or reaction with carbon-based nucleophiles to form carboxylic acids.

The carbon-carbon (C-C) bond is the most fundamental constituent of organic molecules. In order for CO_2 to become a versatile carbon source in the laboratory, it is essential to design efficient catalysts for C-C bond formation from CO_2. Catalytic strategies typically involve insertion of CO_2 into metal-alkyl or -aryl bonds. Such reactions can be divided into two main types: *i*) Substitution reactions involving alkanes, alkenes, alkynes or arenes as substrates and *ii*) Addition reactions to alkenes or alkynes (Fig. 2).

Here we summarize 16 computational studies (from 2010 and onwards) related to the two transition metal-catalyzed C-C bond formation reactions given in Fig. 2. Particular focus is on the proposed mechanisms and the transition state (TS) geometries at the C-CO_2 bond formation step. On basis of the discussed examples for substitution at C_{sp}, C_{sp2}, C_{sp3} and addition at C_{sp} and C_{sp2}, we identify trends connected to transition metal-catalyzed CO_2 activation and fixation into C-C bonds.

2. Review of computational studies

2.1. Substitution at C_{sp}

Copper: In 2010, Lu and co-workers [21] reported the carboxylative coupling of terminal alkynes and allylic chlorides with CO_2 in the presence of IPr-Cu-Cl (Fig. 3). The details of the reaction were computationally investigated by Yuan and Lin in 2014, employing B3P86 together with PCM (DMF solvent) on the full molecular system [22]. The first step of the proposed mechanism is the base-mediated insertion of the terminal alkyne into IPr-Cu-Cl to form the Cu-acetylide intermediate. This intermediate undergoes a

* Corresponding author.
E-mail address: kathrin.hopmann@uit.no (K.H. Hopmann).
[1] These authors contributed equally to this work.

https://doi.org/10.1016/j.jorganchem.2018.02.020

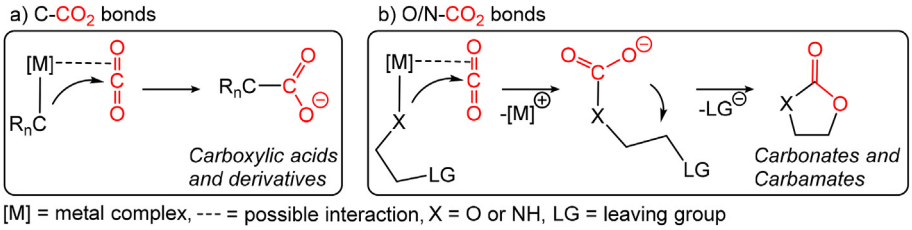

Fig. 1. Two transition metal-catalyzed strategies for the formation of C-CO_2 and O/N-CO_2 bonds.

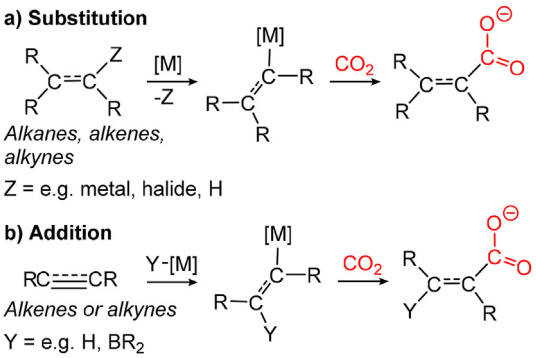

Fig. 2. Two types of C-CO_2 bond formation.

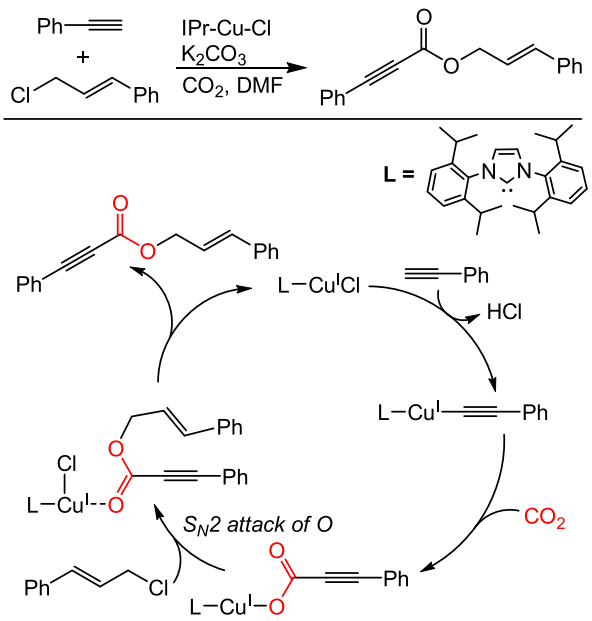

Fig. 3. Mechanism for carboxylative coupling of alkynes and allylic chlorides [21,22].

nucleophilic attack on CO_2 with an activation barrier of 18.6 kcal/mol, leading to formation of a Cu-carboxylate. The TS of the CO_2 insertion step is pictured in Fig. 4, showing no significant interaction between copper and CO_2 (Cu-C_{CO2} distance of 2.94 Å). The third step is rate-determining with a barrier of 24.1 kcal/mol and consists of an SN_2-like attack of the carboxylic oxygen on the allylic chloride, resulting in the dissociation of Cl, which then binds to Cu. An oxidative addition of the allylic chloride was excluded. The authors also computed a cross coupling side reaction, which from

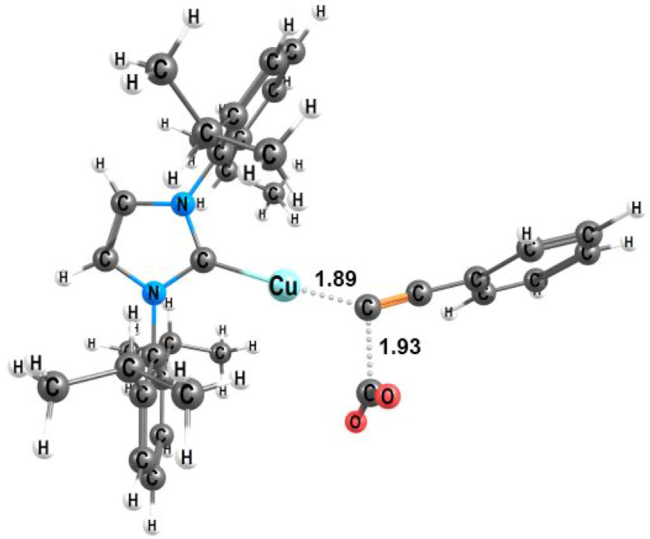

Fig. 4. TS geometry for C_{sp}-CO_2 bond formation with a Cu-(IPr) complex (distances in Å, coordinates from Ref. [22]).

experiment is known to be competitive. Comparing B3P86 with and without the Grimme empirical dispersion correction D2 [23], the authors concluded that pure B3P86 gives an energetic profile that is in better agreement with experiment.

In 2010, Yu and Zhang reported the Cu-catalyzed C-H bond activation and carboxylation of terminal alkynes [24]. Yang et al. studied the CO_2 insertion step of this reaction in 2014 utilizing an NHC ligand possessing two carbenes [25]. Geometries of the full molecular system were optimized with B3LYP in vacuum. The CPCM model (DMF solvent) was employed for computing single point energies of some of the optimized geometries. The authors compared several possible reaction paths, differing with respect to the interaction of CO_2 and Cu with the NHC ligand. Their results predict that the Cu species coordinated by both carbenes of the ligand gives the reaction path with the lowest overall barrier (Fig. 5). The associated CO_2 insertion TS indicates that CO_2 is not interacting with copper (Cu-C_{CO2} distance of 2.84 Å), in line with the observations by Yuan and coworkers (Fig. 4) [22]. The computations also predict formation of a stable off-cycle intermediate with one carbene coordinating to Cu and the other binding to CO_2 (**II**, Fig. 5). Analysis of the energies presented in Ref. [25] indicate that **II** is 4.5 kcal/mol lower in energy than the di-coordinated species **I** (Fig. 5). The barrier for formation of **II** via dissociation of a carbene ligand in **I** was not computed, but based on the energy of an intermediate species, it should be above 9.6 kcal/mol (relative to **I**). The barrier for the on-cycle conversion of **I** to **III** via CO_2 insertion into the metal-substrate bond was computed to 10.3 kcal/mol (relative to **I**). The barriers appear so similar that formation of **II** should not be ignored, as it may either represent an off-cycle

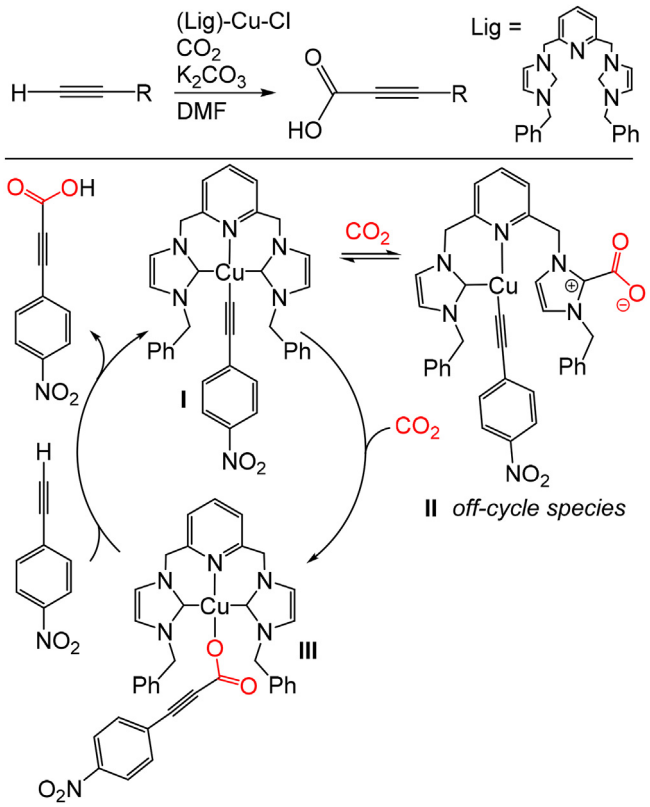

Fig. 5. Proposed mechanism for copper-catalyzed C-H bond activation and carboxylation of terminal alkynes [25].

thermodynamic sink, or the true catalytic species. The latter was excluded by the authors due to the high barrier for insertion of the captured CO_2 of **II** into the metal-substrate bond. However, we recommend to test reaction of an additional *free* CO_2 molecule with **II**, which clearly should be lower in energy than insertion of the captured CO_2. **II** may actually be both an on-cycle species and the resting state of the system.

Copper vs. Silver: In 2017, Velázquez et al. reported a combined experimental and theoretical investigation of the carboxylation of terminal alkynes in presence of NHC-Cu or Ag and a cesium additive (Fig. 7) [26]. Geometry optimizations were performed on the full molecular system under vacuum conditions with B3LYP and the Grimme empirical dispersion correction D3 [27]. The authors concentrated their computational investigation on the CO_2 insertion step of the reaction and found a TS, were the CO_2 is activated by a cesium ion, which is interacting with the sulfonic group of the NHC ligand. Optimized coordinates of the TS were not provided, but the given illustrations indicate that Cu and Ag do not show significant interactions with CO_2. The barriers were similar for the two metals (25.8 kcal/mol for Cu vs. 24.3 kcal/mol for Ag), slightly favouring the Ag complex.

Cu vs Ni vs Rh vs Ir vs Co: In 2016, Vummaleti et al. computed the barrier heights for insertion of CO_2 into different metal-C≡C-Ph complexes [28]. The metals [Cu(I), Ir(I), Ni(II), Rh(I), Co(I)] were bearing COD and IPr ligands [COD = 1,5-cyclooctadiene; IPr = 1,3-bis(isopropyl)-imidazol-2-ylidene]. Geometry optimizations were performed at the BP86 level in vacuum, with single point energy evaluations with M06. The optimized TSs show significantly different distances for the M-C_{alkyl}, C_{alkyl}-C_{CO2}, M-C_{CO2}, and M-O bonds (see Fig. 8 for the Cu-, Ni- and Rh-geometries). The Cu complex shows a C_{alkyl}-C_{CO2} distance of only 1.76 Å, which is significantly shorter than for the related Cu-catalyzed reactions in Figs. 4 and 6. This may be due to the presence of both a COD and an NHC ligand on copper. The CO_2 molecule is positioned 2.75 Å from the metal, indicating a weak interaction at best. A similar geometry is observed for the rhodium system. In contrast, the nickel complex shows metal-CO_2 interactions involving the O atom, and a weak interaction to C (Fig. 8). The computed barriers for the different complexes showed substantial differences, with Ni(II) giving the highest barrier (45.4 kcal/mol) and Cu(I) displaying the smallest barrier (20.8 kcal/mol, Fig. 9). The poor performance of Ni(II) is in line with related findings for substitution at C_{sp2} (*vide infra*).

2.2. Substitution at C_{sp2}

Nickel: In 2012, Tsuji and co-workers reported Ni-$(PPh_3)_2$-catalyzed carboxylation of aryl chlorides (Fig. 10) [29]. Sayyed et al. studied this mechanism computationally in 2013 [30]. The calculations were performed on the full molecular system with B3LYP-D2. Geometries were optimized in vacuum, with PCM (DMI solvent) included as a correction to the electronic energy. The calculations predict that the substrate initially undergoes oxidative addition to nickel, followed by Mn-mediated reduction of Ni(II) to Ni(I) (Fig. 10). CO_2 reacts with the Ni(I) species and then forms a bond to the aryl carbon. The barrier for an alternative reaction pathway involving direct reaction of the Ni(II)-complex with CO_2 was considered too high, i.e. Mn-mediated reduction of nickel to Ni(I) is essential for the reaction to occur. The optimized TS shows a cyclic conformation with substantial interactions between Ni and CO_2 at the C_{sp2}-CO_2 bond formation step (Fig. 10).

Rhodium: In 2006, Iwasawa and co-workers reported the Rh(I)-catalyzed carboxylation of aryl- and alkenylboronic esters [31]. Qin et al. provided a computational investigation in 2014 [32]. The DFT functional PBE0 with PCM was employed. The authors examined the Rh-catalyzed carboxylation of arylboronic esters, involving bidentate rhodium ligands with different electronic properties: a phosphine-based ligand [dppp = 1,3-bis(diphenylphosphino) propane] or the diene ligand COD. The computational analysis supported the previously proposed mechanism (Fig. 11): formation of an Rh-Ph intermediate (**I**), which then interacts with CO_2 to form the Rh-OOCPh species (**II**) through a rate-limiting carboxylation step. At the TS, the CO_2 interacts with the rhodium center through the oxygen and carbon atom in a η^2 binding mode (Fig. 12). The formed carboxylate coordinates either in a monodentate (**IIa**) or a bidentate (**IIb**) fashion (Fig. 11). The complex can then undergo

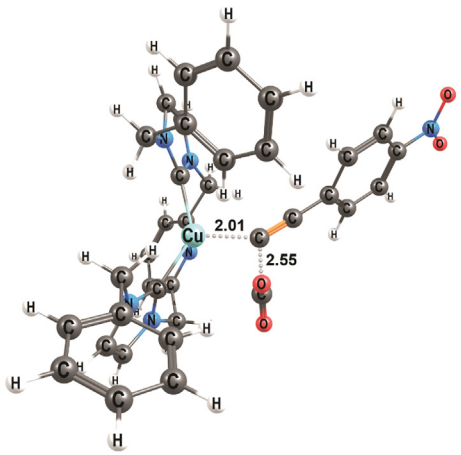

Fig. 6. TS geometry for Cu-catalyzed C_{sp}-CO_2 bond formation (distances in Å, coordinates from Ref. [25]).

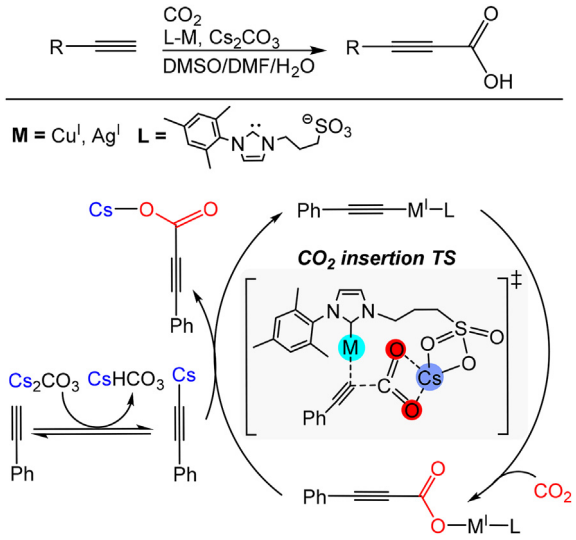

Fig. 7. Proposed mechanism for Cu(I) and Ag(I) catalyzed carboxylation of terminal alkynes (based on [26]).

either a direct transmetallation with an arylbororonic ester substrate to form a carboxylated boron species and regenerate **I**, or proceed via a cesium benzoate (Fig. 11).

With dppp as ligand, the computed barrier was 12.7 kcal/mol. It involved a transformation from a square-planar O-(η^1)-bonded CO_2 to a distorted tetrahedral η^2-coordination. With COD as ligand, the barrier was 17.7 kcal/mol. According to the authors, bidentate phosphines are a better choice due to the larger σ-donor/π-acceptor properties compared to COD.

In 2011, Iwasawa and co-workers reported the direct Rh(I)-catalyzed carboxylation of arenes via chelation-assisted C-H bond activation [33] (Fig. 13). Recently, Lv et al. provided a computational study of this reaction [34]. B3LYP and the SMD model (solvent DMA) were employed. The modelled reaction was the carboxylation of 2-phenylpyridine, which in presence of $[Rh(coe)_2Cl]_2$, a $PMes_3$ ligand, and a methylmetallic reagent forms the desired *ortho*-carboxylated product, alongside a methylated byproduct. The proposed mechanism (Fig. 13) included C-H oxidative addition, CO_2 insertion into the Rh-C(aryl) bond, transmetallation, and methylation.

The authors considered two possible active species of the catalyst, [Rh(I)-Cl] or [Rh(I)-Me], but found that the latter was more likely, due to a lower barrier for the reductive elimination step. The analysis also revealed that $AlMe_2(OMe)$ may act as a Lewis acid, which facilitates the rate-limiting CO_2 insertion step (Fig. 14). For C-C bond formation in the absence of $AlMe_2(OMe)$, the barrier was higher in energy by 6.2 kcal/mol. According to the authors, a favorable interaction between aluminum and CO_2 could make the latter more electrophilic and facilitate its insertion. A possible interaction between $ZnMe_2$ and CO_2 was excluded, as it made both CO_2 coordination and insertion highly disfavored.

Copper: In 2008, Hou and co-workers reported the carboxylation of aryl- and alkenylboronic esters with CO_2 in the presence of IPr-Cu-Cl [35]. Dang et al. investigated this reaction computationally in 2010 [36]. Calculations were performed with B3LYP on a truncated molecular system with the 1,3-diisopropylphenyl groups of the IPr ligand replaced with methyl groups. Optimizations were performed in vacuum, with PCM (THF solvent) single-point

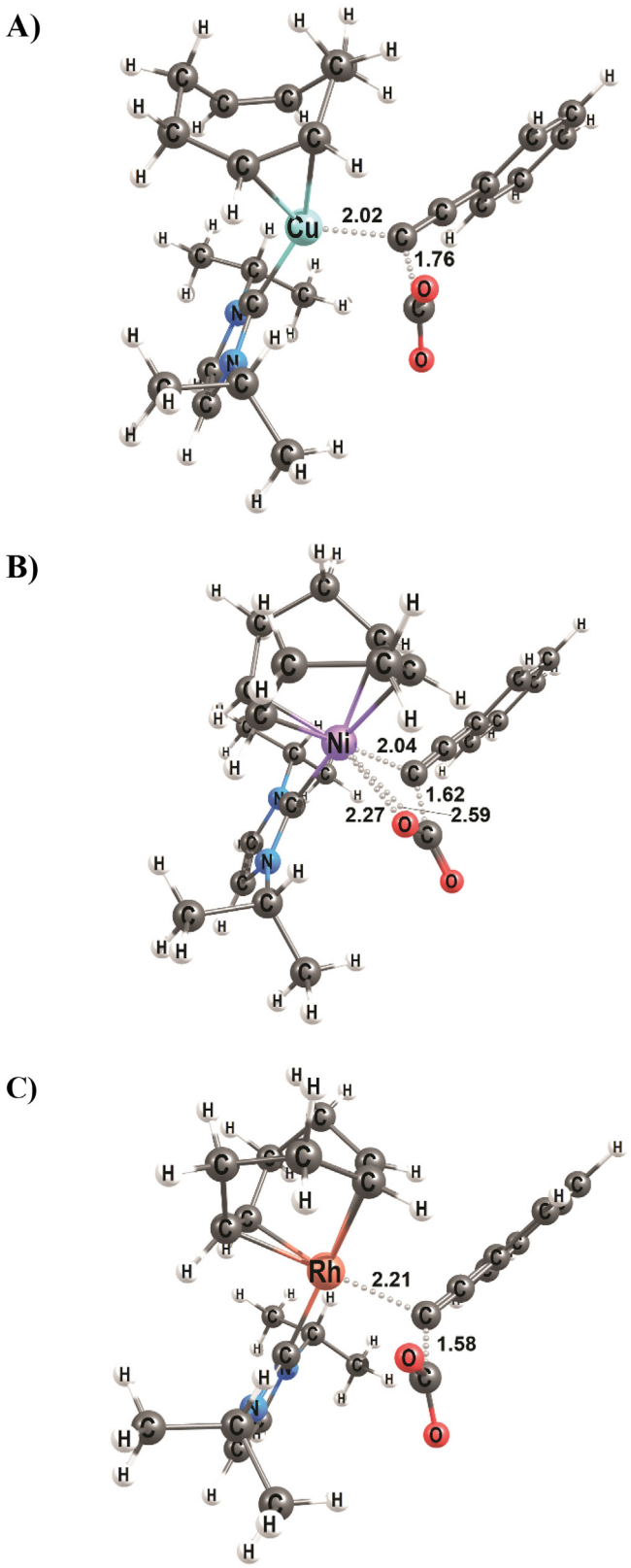

Fig. 8. C_{sp}-CO_2 bond forming TS with metal-(COD)(IPr) complexes, A) Cu(I), B) Ni(II), C) Rh(I) (distances in Å, from coordinates given in Ref. [28]).

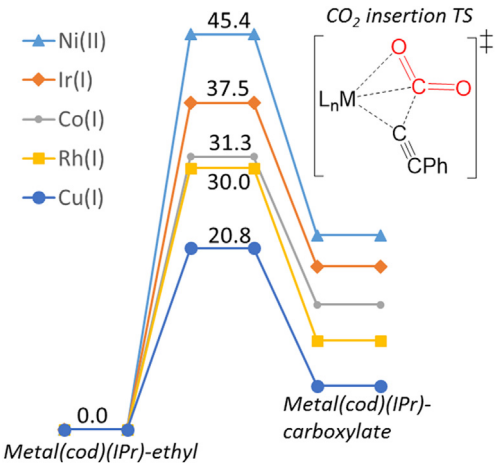

Fig. 9. Computed barriers for C_{sp}-CO_2 bond formation with five metal-(COD)(IPr) complexes (adapted from Ref. [28]).

calculations.

The reaction (Fig. 15) occurs in three steps: the base-mediated formation of the Cu-aryl intermediate, the rate-determining insertion of CO_2 (occurring via a three-membered cyclic TS, Fig. 16), and the regeneration of the active species. The barriers for CO_2 insertion were 25.5 kcal/mol for 4-nitrobenzene and 24.3 kcal/mol for *N,N*-dimethyl-4-aminobenzene. The authors evaluated the effect of charge on the barrier of the CO_2 insertion and found that electron donating ligands lower the barrier. In addition, they compared CO_2 insertion into Cu-C_{sp3}, Cu-C_{sp2} and Cu-C_{sp} bonds for ethyl derivates and found that the barrier is decreasing in the order $C_{sp} > C_{sp3} > C_{sp2}$.

2.3. Substitution at C_{sp3}

Rhodium: In 2011, Ostapowicz et al. reported a computational study on the insertion of CO_2 into the rhodium-ethyl bond of 38 different pincer complexes [37]. The DFT functional B97-D was employed in geometry optimizations and frequency calculations. The computational analysis focused on the interaction between CO_2 and the Rh-pincer complexes prior to insertion, and on the TS for the C-C bond formation step leading to the carboxylate complex. Different binding modes of the CO_2 to the metal center were observed (Fig. 17).

In 30 complexes, the CO_2 molecule coordinated to the metal center through the carbon atom in an η^1-fashion. Only one complex had an η^2-coordinated CO_2 through the C=O bond, while seven complexes show negligible interactions between rhodium and CO_2, with the distances greater than 3.2 Å.

The insertion of CO_2 into the Rh-C bond occurs through a three-membered cyclic TS between Rh, alkyl and CO_2, where the oxygen atom of CO_2 does not interact with the metal (Fig. 18). The activation barriers were calculated as the difference between the energies of the CO_2 adducts and the TSs and their values varied broadly, from 4.0 to 47.3 kcal/mol. Some complexes, e.g. an anionic Rh-pincer-ethyl complex (Fig. 19), showed strong binding to CO_2, yet very low activation barriers for the CO_2 insertion step, implying that no correlation between the calculated binding energies and insertion barriers could be observed. Interestingly, certain complexes did not show any ability to bind CO_2 but still had moderate insertion barriers, implying that pre-coordination of CO_2 to the metal center is not an essential requirement for this reaction. The authors concluded that the nucleophilicity of the alkyl chain is a main factor that affects the heights of the insertion barriers.

Nickel: In 2013, Martin and co-workers reported the Ni-catalyzed carboxylation of a benzyl halide [38]. Efficient transformation was dependent on the presence of Zn and $MgCl_2$. It was proposed that an Ni(I) intermediate is involved (Fig. 20). Sakaki and co-workers studied the putative pathway computationally in 2014 [39]. The mechanism is very similar to the C_{sp2} case (Fig. 10), but involves an $MgCl_2$ molecule, which interacts with CO_2 (Fig. 20, right). Calculations were performed at the B3LYP-D2 level of theory on the full molecular system, with geometries optimized in vacuum. Single point energy calculations included IEFPCM (DMF solvent). The study concluded that $MgCl_2$ plays a crucial role during the mechanism in activating CO_2. In absence of $MgCl_2$, the C-CO_2 bond formation barrier is computed to be 12 kcal/mol higher.

2.4. Addition at C_{sp}

Copper: In 2011, Tsuji and co-workers [40] reported the Cu-catalyzed hydrocarboxylation of alkynes with hydrosilanes (Fig. 21). The mechanism of the reaction was investigated in 2012

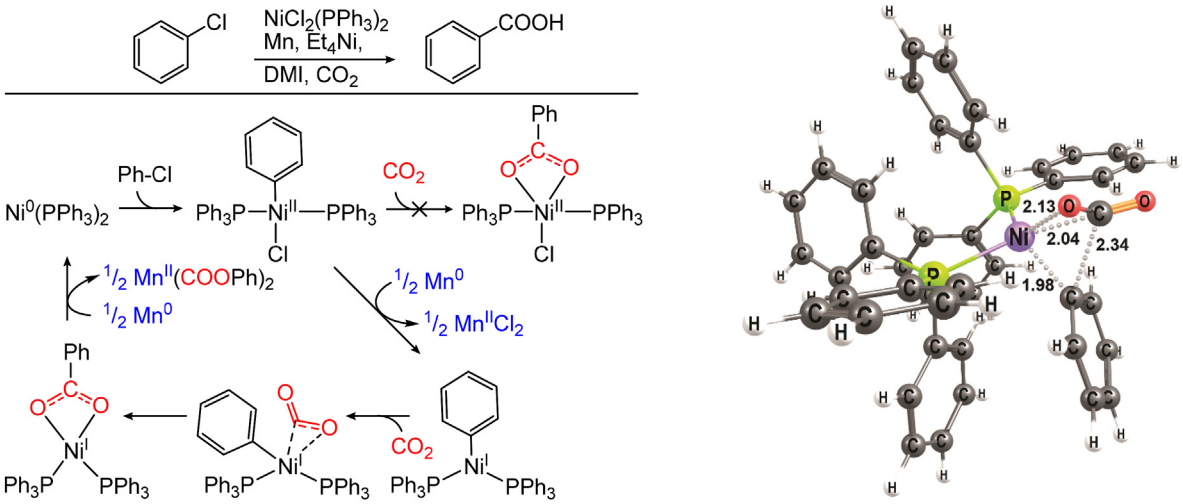

Fig. 10. Left: Ni-catalyzed carboxylation of aryl chloride and proposed mechanism [29,30]. Right: Optimized geometry for the CO_2 insertion TS of Ni(PPh_3)$_2$-mediated carboxylation of an arene (distances in Å, based on coordinates in Ref. [30]).

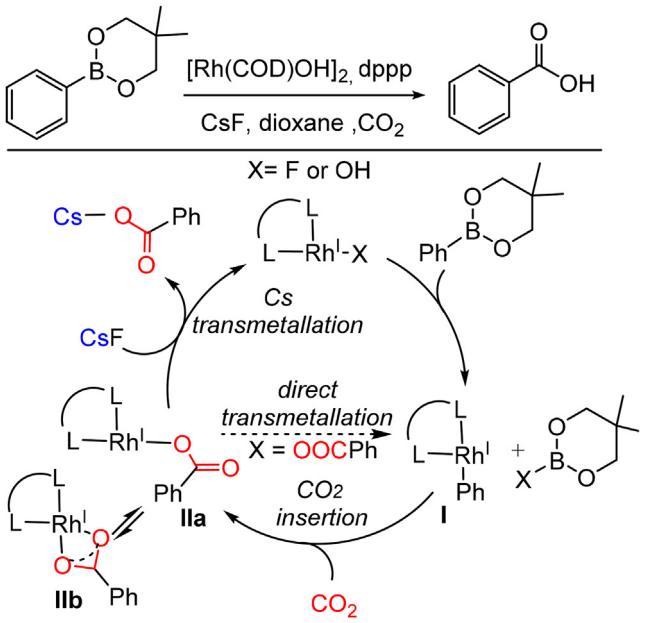

Fig. 11. Rh(dppp)-catalyzed carboxylation of alkyl-boronic esters and proposed mechanism (based on [32]).

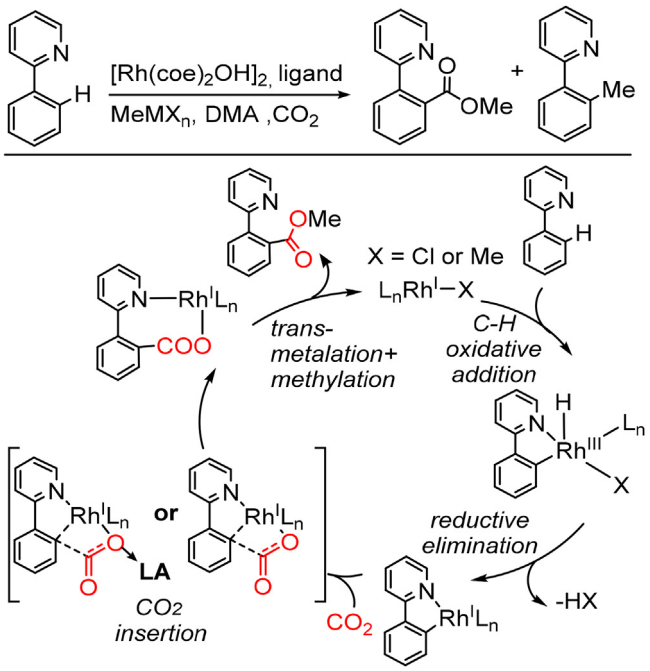

Fig. 13. Direct Rh(I)-catalyzed carboxylation of arenes with CO_2 and proposed mechanism (based on [33,34]).

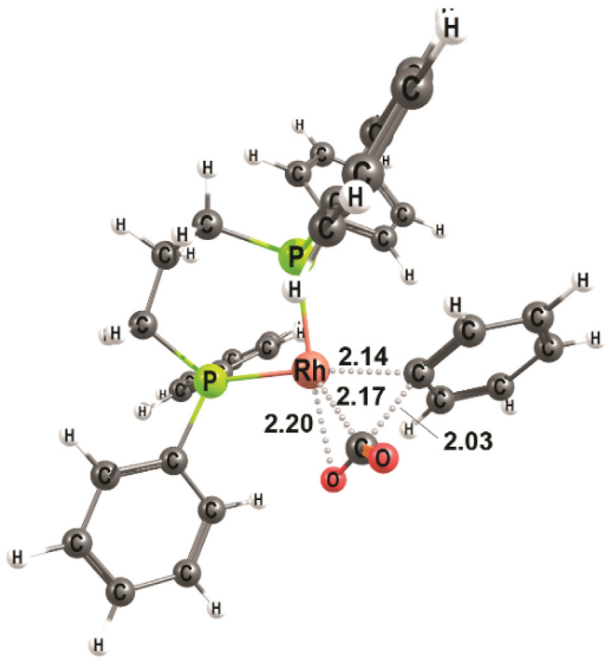

Fig. 12. C_{sp2}-CO_2 bond forming TS with a Rh-(dppp) complex (distances in Å, based on coordinates from Ref. [32]).

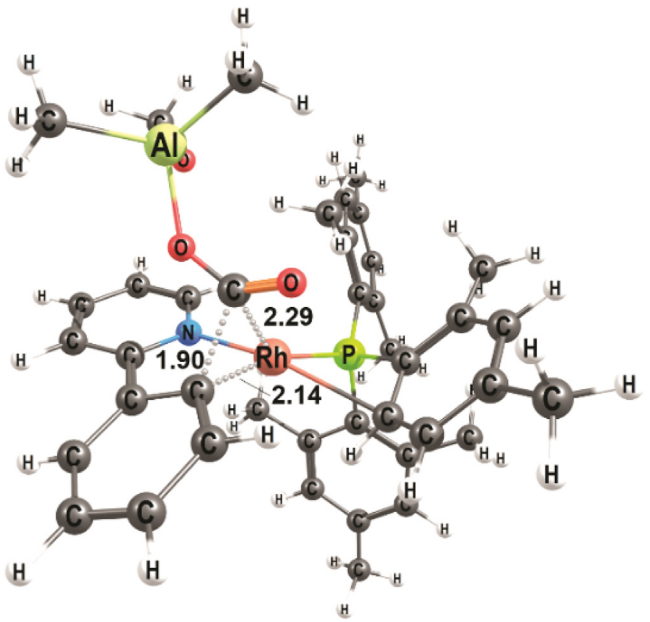

Fig. 14. Rh/Al-catalyzed carboxylation of 2-phenylpyridine (distances in Å, coordinates from Ref. [34]).

by Wang et al. [41] with emphasis on the regioselectivity of asymmetric alkynes, and in 2013 by Fan et al. [42], with focus on the full reaction cycle including putative side reactions. Different NHC ligands were employed, matching the experimental setup for the studied substrates. Both groups optimized geometries with B3LYP in vacuum. Energies were calculated with MP2 (Wang) and B3LYP (Fan) and PCM (Wang: *n*-heptane, Fan:1,4-dioxane solvent) was included. Both groups truncated the system by replacing the 1,3,5-trimethylphenyl groups of the NHC with methyl groups.

The computed reaction path has three major steps (Fig. 21). First the insertion of the alkyne into the (NHC)-Cu-H species, forming an alkenyl, second the insertion of the CO_2 into the Cu-C bond (Fig. 22) and third the regeneration of the active species via reaction with a hydrosilane. Wang et al. working on asymmetric alkynes, found that the regioselectivity is determined by first step of the reaction, the insertion of the alkyne into (NHC)-Cu-H. While this step is not rate-determining for the overall reaction, it is decisive for the selectivity due to its irreversibility. The authors calculated the barrier of the first step for three alkynes, observing similar preferred regioisomers. In Wang's calculations, the insertion of CO_2

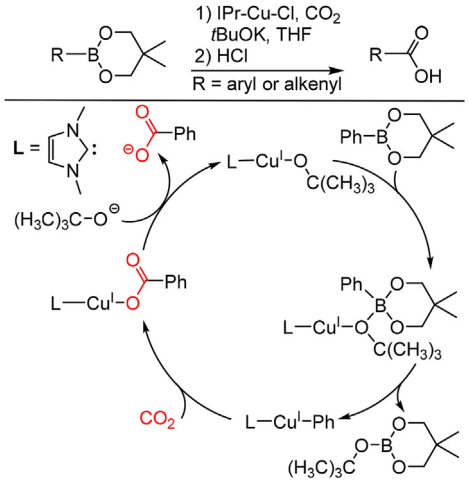

Fig. 15. Proposed mechanism for Cu-catalyzed carboxylation of arylboronate esters with CO_2 (based on [35,36]).

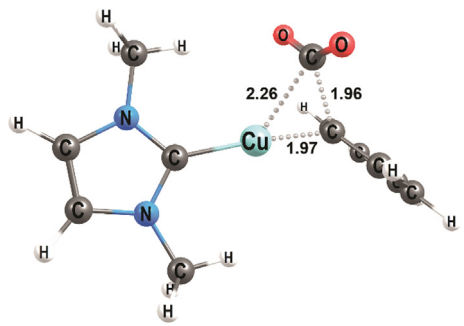

Fig. 16. TS for Cu-catalyzed carboxylation of aryl-boronate esters (distances in Å, coordinates from Ref. [36]).

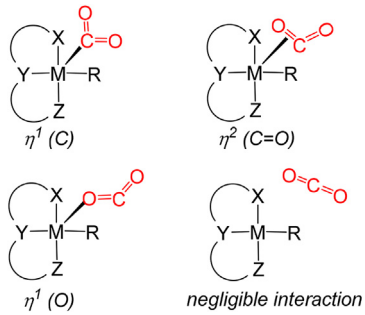

Fig. 17. Interaction modes of CO_2 with metal-pincer complexes prior to CO_2 insertion [adapted from Ref. [37]].

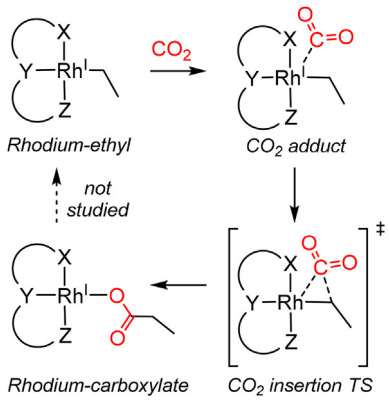

Fig. 18. Schematic representation of the CO_2 insertion into Rh(I)-pincer-ethyl complexes [adapted from Ref. [37]].

is rate determining [41], whereas Fan predicted it to be the regeneration of the catalyst [42]. In addition to the alkyne hydrocarboxylation, Fan et al. investigated three potential side reactions: silacarboxylation of alkynes, hydrosilylation of alkynes, and hydrosilylation of CO_2. None of these is observed in experiment. It was concluded that silacarboxylation is endergonic and hydrosilylation of alkynes has an inaccessibly high reaction barrier. Hydrosilylation of CO_2 appears feasible based on the computed energies, but was suggested to be unlikely to occur, as CO_2 insertion into a Cu-hydride is heterogeneous in nature compared to homogeneous insertion of an alkyne into Cu-H [42].

2.5. Addition at C_{sp2}

Rhodium: In 2012, Ostapowitz et al. reported a computational investigation of a hypothetical Rh-catalyzed hydrocarboxylation of ethene with CO_2 and H_2 [43]. From their previous investigation [37], three Rh-pincer complexes with different electronic properties were chosen as potential catalysts (Fig. 23). The functional B97-D was employed. In the proposed mechanism (Fig. 24), a rhodium hydride species was used as a starting point. The insertion of ethene gives a Rh-alkyl intermediate, which interacts with CO_2 through a three-membered cyclic TS (Fig. 25) to form a carboxylate complex. The activation barrier for the C-CO_2 bond formation step of the anionic complex **C** was found to be 12.3 kcal/mol and for the corresponding complexes **A** and **B**, 24.5 kcal/mol and 36.1 kcal/mol, respectively. Subsequently, the hydrogenolytic cleavage of the carboxylate complex leads to the carboxylic acid (Fig. 24). The authors found four possible pathways for the hydrogenolysis: *i*) a σ-bond metathesis via a four-membered or *ii*) six-membered transition state, *iii)* an exchange of the carboxylate for H_2 followed by heterolytic cleavage, and *iv)* a classical oxidative addition/reductive elimination. The computed energy profile showed that each of the three complexes (**A-C**, Fig. 23) gave different hydrogenolysis pathways, which was attributed to the different electronic properties of the pincer ligands. The σ-bond metathesis via a six-membered TS was preferred for complex **A**. For **B**, only a pathway via oxidative addition of H_2 was found. For **C**, a σ-bond metathesis pathway was not located and it was concluded that the carboxylate may be replaced by H_2, followed by heterolytic H_2 cleavage.

From the energy profiles, the anionic complex **C** was proposed to be the most promising candidate, with stable intermediates and overall barriers below 13 kcal/mol. The enhanced electron density at the metal center of **C** leads to a very nucleophilic alkyl intermediate that can easily interact with the electrophilic CO_2. The authors concluded that an electron-rich rhodium center is important for successful hydrocarboxylation and prevention of the major competing reaction, the hydrogenation of olefins.

Nickel: In 2008, Rovis and co-workers reported a seminal study on nickel-catalyzed hydrocarboxylation of substituted styrenes [44] (Fig. 26). The details of this reaction were studied computationally by Yuan and Lin in 2014 [45]. Calculations were performed on the full molecular model with B3LYP and a PCM solvent model. The work compared two mechanisms: an oxidative coupling mechanism and a nickel-hydride pathway (Fig. 26). Both mechanisms set out from a Ni(DBU)$_2$-CO_2 species. In the oxidative coupling, reaction with styrene leads to formation of an

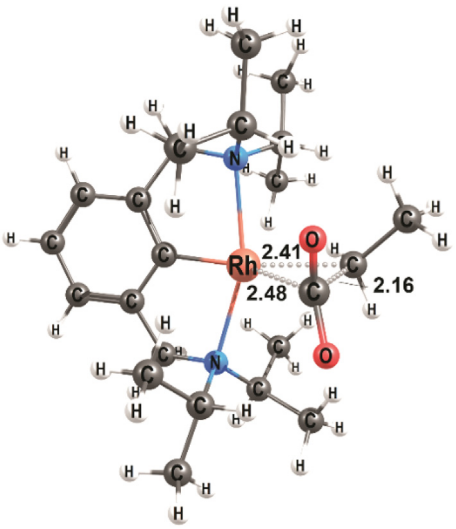

Fig. 19. CO_2 insertion TS with an anionic Rh-pincer-ethyl complex (distances in Å, coordinates from Ref. [37]).

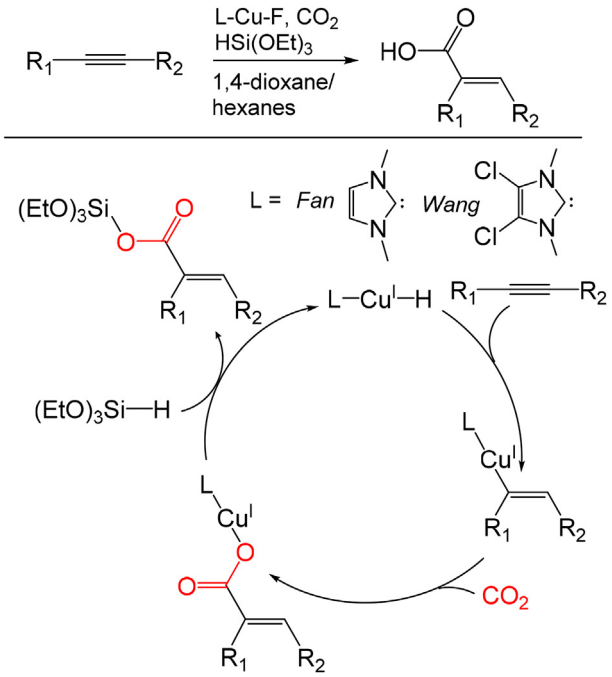

Fig. 21. Mechanism for the copper-catalyzed hydrocarboxylation of alkynes (adapted from Refs. [41,42]).

energetically low-lying metallacycle species. According to the authors this was unlikely to take place in reality, as it would result in a too high barrier for the hydrocarboxylation reaction. The metallacycle mechanism also predicts carboxylation of the styrene β-carbon to be energetically preferred, in disagreement with experiment [44]. The nickel-hydride mechanism gave a reasonable barrier (but only if it is assumed that formation of a metallacycle can be avoided) and the correct regioselectivity, resulting in the α-carboxylated product. The overall barrier for the Ni-H mechanism was 19.8 kcal/mol relative to a $Ni(DBU)_2$-CO_2 species, with hydride transfer to the β-carbon and subsequent carboxylation of the α-carbon exhibiting identical barriers. At the carboxylation TS, the CO_2 molecule interacts both with Ni and the Zn additive (Fig. 27). When the computational protocol was augmented with the empirical dispersion corrections D3, formation of the metallacycle was strongly preferred, but the authors considered this an incorrect result. In our opinion, this system deserves additional theoretical and experimental studies to elucidate if a metallacycle intermediate maybe be formed, possibly as an off-cycle species to the nickel-hydride pathway.

Palladium: In 2015, Wu and co-workers reported a computational investigation of the insertion of CO_2 into a (PSiP) palladium allyl bond to form β,γ−unsaturated carboxylic acids [46], originally reported by Takaya and Iwasawa [47]. The functional M06 was employed for the calculations, with the IEFPCM model (solvent DMF) added as single point calculations. In the proposed mechanism (Fig. 28), a palladium hydride intermediate is formed in the presence of $AlEt_3$. Next, insertion of allene forms the η^1-allyl palladium complex, which then interacts with CO_2 to form a

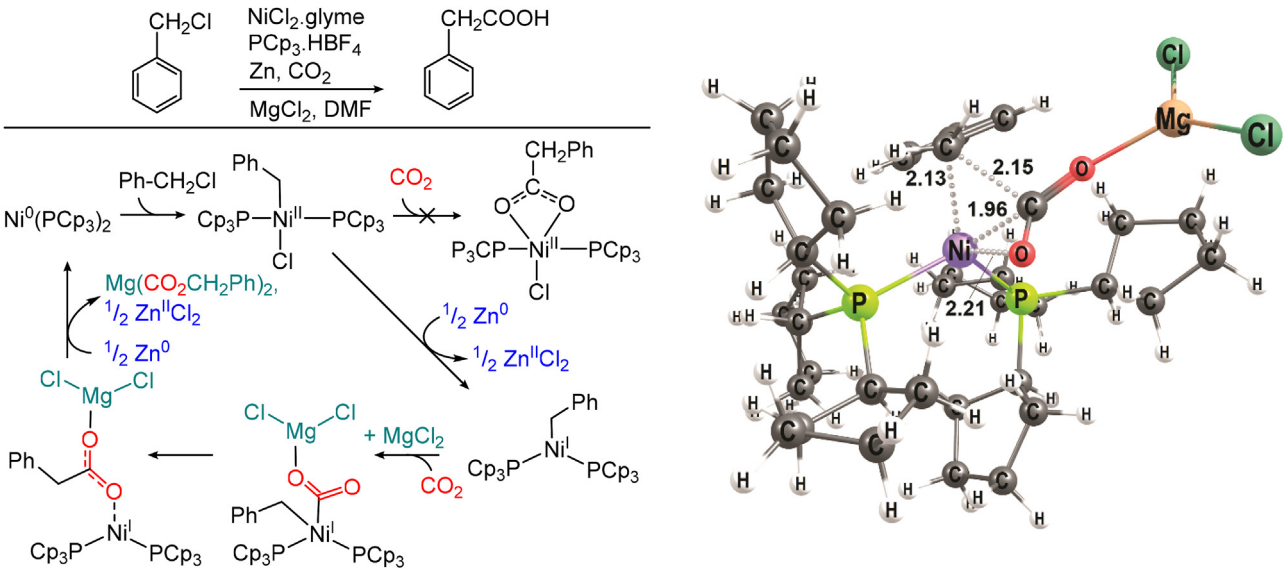

Fig. 20. Left: Ni-catalyzed carboxylation of benzyl chloride and proposed mechanism [38,39]. $MgCl_2$ accelerates the CO_2 insertion. Right: Optimized geometry for the CO_2 insertion step (distances in Å, based on coordinates in Ref. [38]).

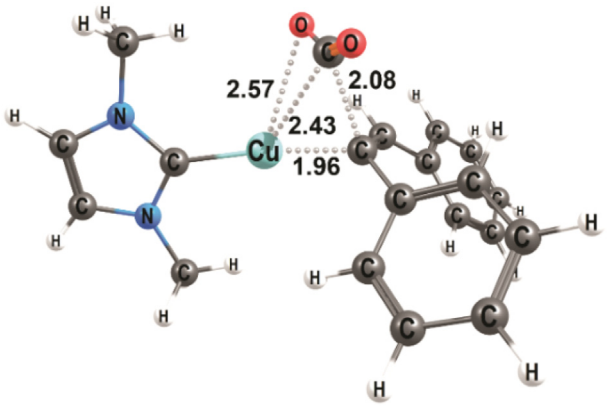

Fig. 22. CO_2 insertion TS in the Cu-catalyzed hydrocarboxylation of a symmetrical alkyne (distances in Å, based on coordinates in Ref. [42]).

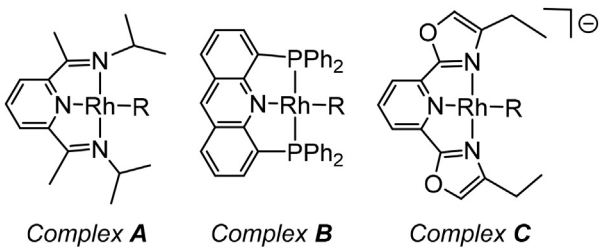

Fig. 23. Rh-catalysts employed in the theoretical study of a hypothetical hydrocarboxylation reaction [43].

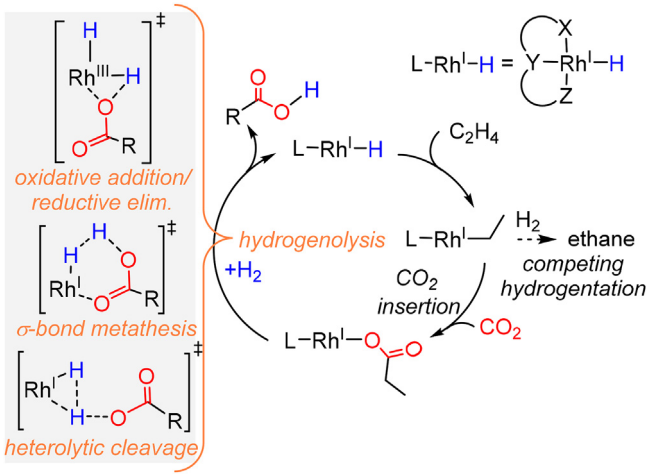

Fig. 24. Proposed mechanism for the direct hydrocarboxylation of ethene with CO_2 and H_2 (based on [43]).

palladium–carboxylate intermediate. Finally, a transmetallation and β-H-elimination regenerates the palladium hydride.

Three possible CO_2 insertion modes were considered: *i)* a direct insertion of CO_2 into the Pd-C bond (leading to carboxylation of the terminal carbon), *ii)* a metallo-ene mode, where the substituted carbon of the double bond reacts with CO_2 via a six-membered TS and *iii*) an S_E2 type reaction, which lacks the CO_2-Pd interaction seen in the metallo-ene mode. The metallo-ene mode (Figs. 28 and 29) was found to be most favorable, with an activation barrier of 21.1 kcal/mol. The computed results were in agreement with the major product observed in experiments. It can be noted that there

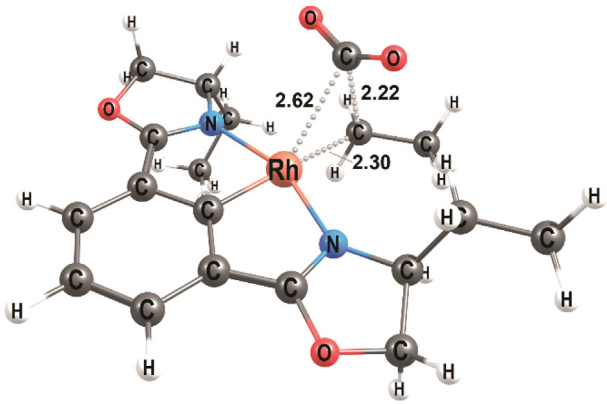

Fig. 25. CO_2 insertion TS in the Rh-catalyzed hydrocarboxylation of ethene (complex **C**, distances in Å, figure prepared from optimized coordinates in Ref. [43]).

exist several earlier mechanistic studies on Pd-catalyzed CO_2 insertion into allylic bonds [48], for a detailed discussion of these see Ref. [19].

Copper: In 2016, Popp and co-workers reported a regioselective copper-catalyzed boracarboxylation of styrenes with CO_2 and B_2pin_2 [49]. The details of the reaction and the effect of the ligands were investigated by Lv et al. in 2017 [50] (Fig. 30). The calculations were performed on full molecular systems with B3LYP in vacuum. Single point energies were acquired with M06 and a SMD model (THF solvent). Icy-Cu-Bpin was suggested as the active species, and the results show a clear preference for the addition of Cu at the α-carbon (barrier of 11.1 kcal/mol vs 22.1 kcal/mol for the β-carbon). The rate-limiting step is the insertion of the CO_2 (barrier of 20.1 kcal/mol), which occurs through a three-membered cyclic TS involving Cu and the two reacting carbon atoms (Fig. 31). Additionally, the authors compared several ligands and concluded that for NHC and biphosphine ligands, the reactivity is determined by the bulkiness and the electronic effects, while for monophosphine ligands, the electron donation ability is dominant.

3. Trends

From the discussed computational studies on C-CO_2 bond formation, some trends can be noted. It should be remembered, however, that due to the medium number of systems included here (18, Table 1) it is not possible to identify such trends with certainty.

Metal-CO_2 interactions and TS geometries: CO_2 is an inert molecule, and it may be expected that its participation in C-C bond formation requires activation of CO_2 by the involved metal catalysts. Such an activation would be expected to occur through direct interactions of CO_2 and the metal. However, the examples discussed here display a variety of different scenarios, ranging from strong metal-CO_2 interactions to no interactions at all. For most of the systems, the overall geometric configuration of the TS is fairly similar, showing three-membered cyclic arrangements involving the metal, and the two reacting carbon atoms (Fig. 32A), where CO_2 interacts with the metal through the C atom (Figs. 8, 14, 16, 19, 25 and 27) or through both C and O (Figs. 10, 12, 20 and 22). At the TS, the CO_2 molecule is typically bend, with angles of 148° down to 117° and exhibits elongated C-O bond lengths (1.20–1.30 Å, Table 1), compared to a free CO_2 molecule (O-C-O 180°, C-O 1.16 Å) [51]. Some trends in interactions and geometries can be observed for the different metals:

- For copper catalysts, CO_2 interacts strongly with the metal and forms three-membered cyclic TSs during bond formation to C_{sp3}

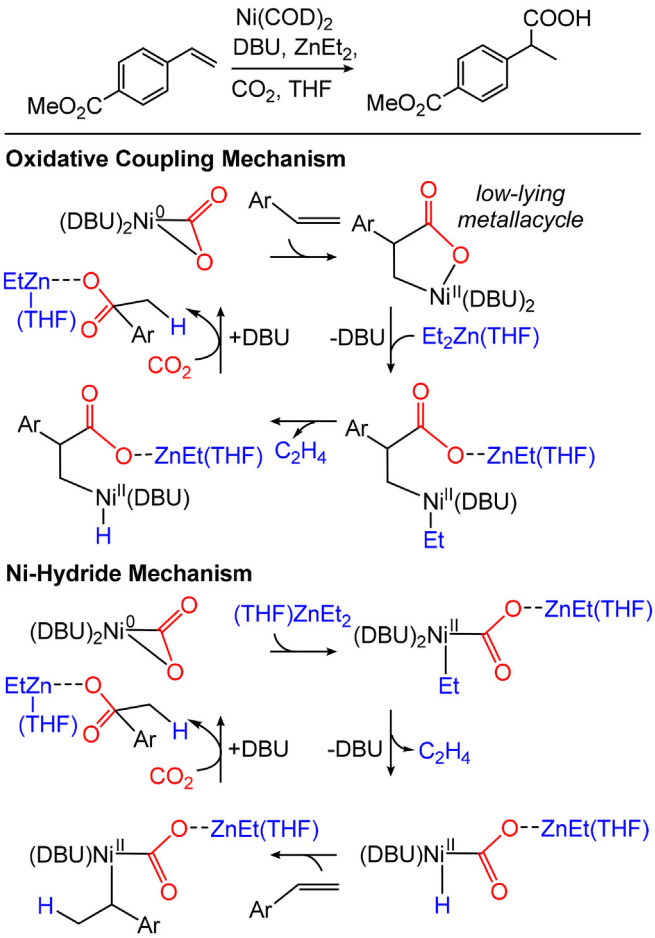

Fig. 26. Ni-catalyzed hydrocarboxylation of styrenes [44] and studied mechanisms [45] (drawn with carboxylation of the α-carbon).

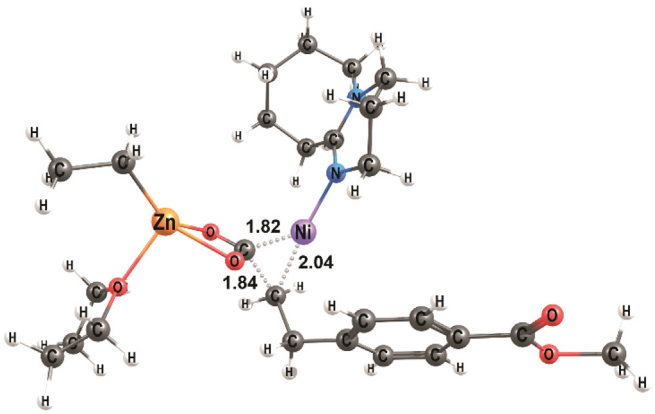

Fig. 27. TS geometry for Ni/Zn-mediated carboxylation of a styrene (distances in Å, coordinates from Ref. [45]).

and C_{sp2} atoms [19,36,41,50], but not for reaction with C_{sp}, where no CO_2-metal interaction is seen [22,25,28] (Figs. 4, 6, 8), resulting in an acyclic TS (Fig. 32B). Based on the Cu-CO_2 bond lengths at the TS (Table 1), it is concluded that the strength of the interaction of CO_2 with Cu depends on the type of nucleophile and has the order $C_{sp3} > C_{sp2} \gg C_{sp}$.

- For nickel-based systems, CO_2 coordination to the metal prior to the carboxylation step may be observed (Figs. 10, 20 and 26)

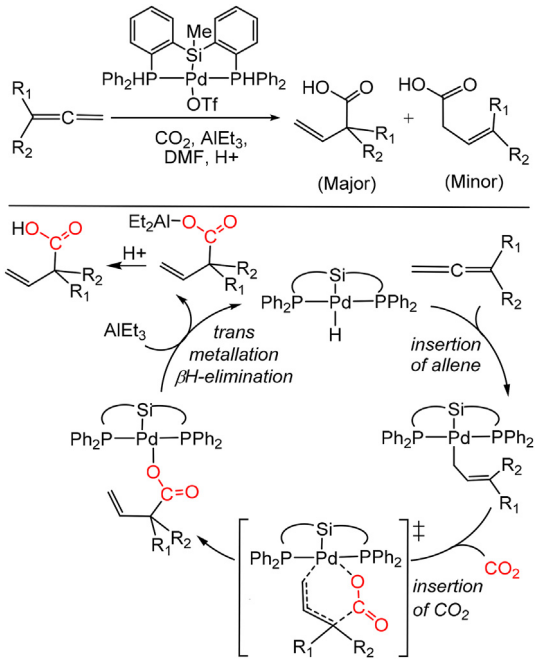

Fig. 28. Pd-catalyzed hydrocarboxylation of an allene with CO_2 and proposed metallo-ene mechanism [46].

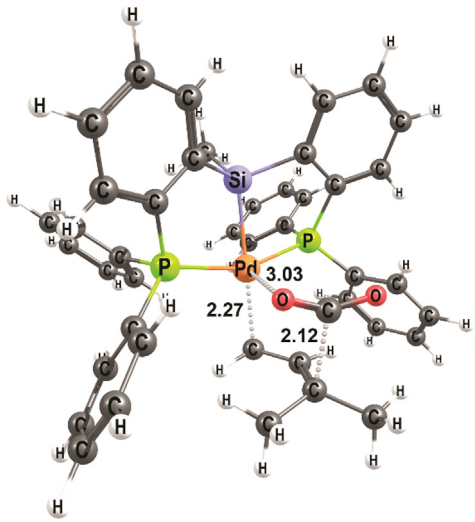

Fig. 29. TS geometry for Pd-catalyzed carboxylation of an allene (distances in Å, coordinates in Ref. [46]).

[30,39,45]. The C-C bond formation involves three-membered cyclic TSs, with binding of CO_2 to the metal through both C and O (Figs. 8, 10 and 20) [22,28,30]. If another metal additive interacts with O, only the C-atom may interact with nickel (Fig. 27) [39]. It can be noted that at least one exception has been reported, proposing no interaction of CO_2 with nickel [52].

- For rhodium, CO_2 interaction with the metal may occur prior to the C-C bond formation TS, however, the strength of such an interaction does not correlate with subsequent barriers [37]. Based on the limited data for rhodium, insertion of CO_2 into a Rh-C_{sp} bond involves no Rh-CO_2 interaction (Fig. 8) [28], as also observed for Cu. Insertion into Rh-C_{sp2} bonds occurs in a η^2-fashion, where both C and O atoms coordinate to the metal

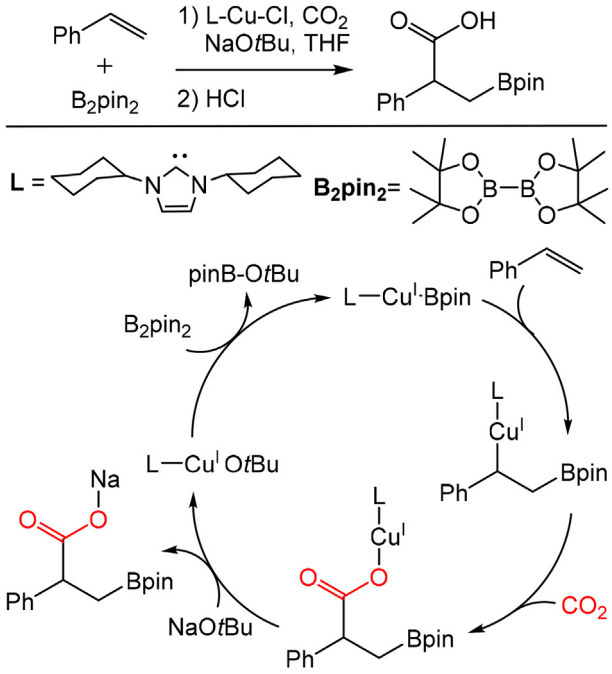

Fig. 30. Mechanism for the copper-catalyzed boracarboxylation of a styrene (adapted from Ref. [50]).

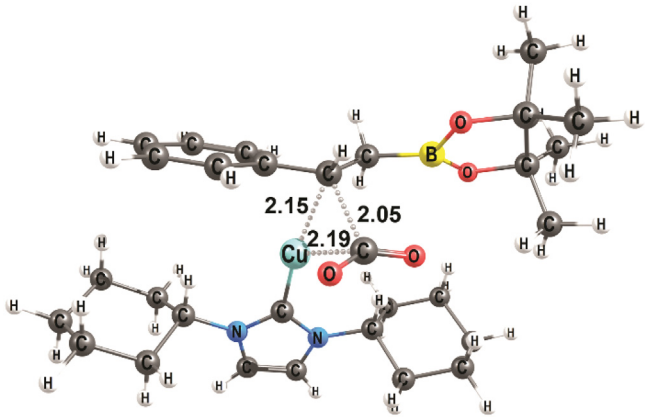

Fig. 31. CO_2 insertion TS in the Cu-catalyzed boracarboxylation of styrene (distances in Å, coordinates from Ref. [50]).

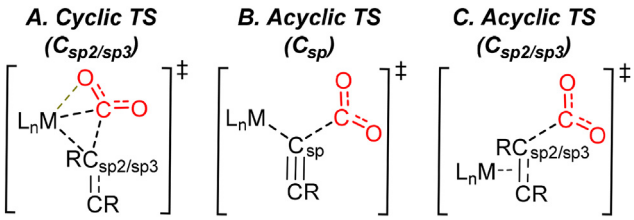

M = Cu, Rh, Ni [30,32,34,36,37,39,41,43,50]

M = Cu, Rh [22,25,28]

M = Pd, Ni, Rh [47,52,53]

Fig. 32. Trends in TS geometries for C-CO_2 bond formation (references in brackets). Most studies report **A**, except for bonding to C_{sp}, where **B** is reported. **C** has been proposed a few times and should be tested more widely.

(Fig. 12) [32]. Insertion into a Rh-C_{sp3} bond takes place through a three-membered cyclic TS, where CO_2 interacts with Rh only via the carbon atom [37,43] (Figs. 19 and 25). However, it can be noted that in a recent investigation of Rh-catalyzed hydrocarboxylation with CO_2, we showed that during C_{sp3}-CO_2 bond formation, CO_2 interacts neither with rhodium nor with a zinc additive, but prefers to remain unbound and to perform a back-attack on the substrate [53] (Fig. 32C). Given that a cyclic TS conformation as shown in Fig. 32A generally may be expected, it is not certain that all computational studies evaluated acyclic conformations such as Fig. 32C. We recommend to always evaluate multiple TS geometries for C-CO_2 bond formation to ensure that the preferred interaction mode is identified. It is also interesting to note that the acyclic conformation indicates that the metal plays no role in the activation of CO_2, but only in the activation of the nucleophile.

Energetic considerations: In the discussed examples, the CO_2 insertion is generally rate-limiting [28,30,32,34,36,41]. It is not possible to conclude that one metal provides lowest barriers, however, it appears that Cu(I) generally gives feasible barriers, whereas Ni(II) may not be good for C-C bond formation with CO_2 [28,30,39]. All of the presented Cu-complexes use NHC ligands but as Lv et al. indicated, other ligands, like e.g. phosphine, can also yield low activation barriers [50]. Despite the good performance of NHC ligands, the interaction of CO_2 with free carbenes can lead to energetically low-lying off-cycle intermediates [45]. For rhodium, bidentate phosphine ligands appear to give lower barriers than COD [32], and anionic pincer ligands appear better than neutral ligands [43].

Several studies suggest that Lewis acid additives (e.g. Al, Mg) through interaction with CO_2 may reduce the barrier for C-C bond formation (Figs. 14 and 20) [34,39]. An interaction with Zn may also occur [35,45], but this may not be beneficial [35].

Computational protocols: All studies reviewed here employed DFT, which provides a good compromise between speed and accuracy, when computing organometallic species. The feasibility of DFT is reflected by the fact that the majority of studies reported calculations on full molecular systems, i.e. without truncating the catalyst or substrate [22,25,26,30,45,50]. However, surprisingly often, geometry optimizations were done in vacuum, and solvent corrections were only included to the energy [25,27,28,30,36,39,41,42,50]. Most studies added dispersion corrections (via a Grimme correction [23] or via a functional that is parametrized to reproduce dispersion, e.g. M06 [54]) [26,28,30,39,43,50], but it can be noted that two studies concluded that dispersion corrections gave results that are in disagreement with experiment [22,45]. This is not in line with the general experience in the field, which shows that dispersion corrections provide more accurate reaction energies [55]. We suggest that if agreement with experiment is poor, it may point to that the mechanism occurs in a different manner than what was computed. For example, if computations predict a stable off-cycle species, then rather than ascribing this to incorrect predictions by the computational protocol [45], it should be considered if an alternative mechanism may be able to incorporate this state [56].

4. Conclusions

We have reviewed computational studies that investigated transition metal-catalyzed C-C bond formation with CO_2. Although the overall mechanisms are dependent on the substrate at hand, the reported TS geometries for the CO_2 insertion steps show similar features, mostly displaying three-membered cyclic rings.

Table 1
Geometrical parameters of reported transition states for C-CO_2 bond formation.

	Metal-complex at TS	Reaction with	C-O_A Å	C-O_B Å	O-C-O °	C_{Alkyl}-CO_2 Å	M-C_{Alkyl} Å	M-C_{CO2} Å	M-O_{CO2} Å	Ref.
Cu	Cu(I)-NHC	C_{sp}	1.20	1.20	145	1.93	1.89	2.94	3.41	[22]
	Cu(I)-NHC(2 carbenes)	C_{sp}	1.20	1.21	145	1.93	2.01	2.84	3.26	[25]
	Cu(I)-NHC-COD	C_{sp}	1.22	1.23	140	1.76	2.02	2.75	3.05	[28]
	Cu(I)-NHC-SO_3/Cs	C_{sp}	NA[a]	NA	NA	1.83	1.93	NA	NA	[26]
	Cu(I)-NHC	C_{sp2}	1.19	1.21	146	2.08	1.96	2.43	2.57	[19]
	Cu(I)-NHC	C_{sp2}	1.20	1.22	142	1.95	1.97	2.34	2.56	[41]
	Cu(I)-NHC	C_{sp2}	1.21	1.22	142	1.96	1.97	2.26	2.66	[36]
	Cu(I)-NHC	C_{sp3}	1.22	1.22	140	2.05	2.15	2.19	2.57	[50]
Ni	Ni(II)-NHC-COD	C_{sp}	1.22	1.27[b]	134	1.62	2.04	2.59	2.27	[28]
	Ni(I)-$(PPh_3)_2$	C_{sp2}	1.20	1.24	143	2.32	1.98	2.04	2.13	[30]
	Ni(I)-$(PCp_3)_2$/$MgCl_2$	C_{sp3}	1.24	1.25[b]	133	2.15	2.13	1.96	2.21 (Ni-O) 1.94 (Mg-O)	[39]
	Ni(II)-DBU/Zn(Et)(THF)	C_{sp3}	1.30[b]	1.31[b]	117[c]	1.84	2.04	1.82	2.67 (Ni-O) 2.08 (Zn-O)	[45]
Rh	Rh(I)-NHC-COD	C_{sp}	1.24	1.26	133	1.58	2.21	2.87	2.89	[28]
	Rh(I)-dppp	C_{sp2}	1.20	1.25	141	2.03	2.14	2.17	2.20	[32]
	Rh(I)-$PMes_3$/$AlMe_2OMe$	C_{sp2}	1.21	1.27[b]	134	1.90	2.14	2.29	2.86 (Rh-O) 1.91 (Al-O)	[34]
	Rh(I)-pincer (-)	C_{sp3}	1.22	1.22	141	2.22	2.30	2.62	3.18	[43]
	Rh(I)-pincer (-)	C_{sp3}	1.23	1.23	134	2.16	2.41	2.48	3.06	[37]
Pd	Pd(II)-PSiP	C_{sp2}	1.20	1.20	148	2.12	3.15	3.73	3.03	[47]

[a] NA = not available.
[b] Elongated due to M-O-C_{CO2} interaction, where M = Zn, Mg, Al or Ni.
[c] Both O of CO_2 coordinated to Zn.

Exceptions are reactions with C_{sp} atoms, where acyclic TS geometries are reported, where no metal-CO_2 interactions are observed. We propose that also for reaction with $C_{sp2/sp3}$ atoms, acyclic TS geometries should be evaluated more widely. The insights discussed here deepen the understanding of C-CO_2 bond formation and may be relevant for designing novel CO_2-incorporation reactions.

Competing interests

The authors declare no competing interests.

Acknowledgements

This work has been supported by the Research Council of Norway through a FRINATEK grant (No. 231706) and a Centre of Excellence Grant (No. 262695), by the Tromsø Research Foundation (No. TFS2016KHH), and by NordForsk (No. 85378) and the members of the *Nordic Consortium for CO_2 Conversion* (UiT – The Arctic University of Norway, Uppsala University, Stockholm University, KTH Royal Institute of Technology, Aarhus University, University of Oslo, University of Bergen, Helsinki University, University of Iceland).

References

[1] Q.-W. Song, Z.-H. Zhou, L.-N. He, Green Chem. 19 (2017) 3707–3728.
[2] X.-F. Wu, F. Zheng, Top. Curr. Chem. (Z) 375 (2017) 4.
[3] L. Zhang, Z. Hou, Curr. Opin. Green Sustain. Chem. 3 (2017) 17–21.
[4] J. Vaitla, Y. Guttormsen, J. Mannisto, A. Nova, T. Repo, A. Bayer, K.H. Hopmann, ACS Catal. 7 (2017) 7231–7244.
[5] M. Börjesson, T. Moragas, D. Gallego, R. Martin, ACS Catal. 6 (2016) 6739–6749.
[6] R. Hua, S. Roy, in: I. Karamé (Ed.), Recent Advances in Organocatalysis, InTech, 2016, https://doi.org/10.5772/63096.
[7] E. Kirillov, J.-F. Carpentier, E. Bunel, Dalton Trans. 44 (2015) 16212–16223.
[8] Q. Liu, L. Wu, R. Jackstell, M. Beller, Nat. Commun. 6 (2015) 5933.
[9] D. Yu, S.P. Teong, Y. Zhang, Coord. Chem. Rev. 293 (2015) 279–291.
[10] A.-H. Liu, B. Yu, L.-N. He, Greenhouse gases, Sci. Technol. 5 (2015) 17–33.
[11] M. Ian Childers, J.M. Longo, N.J. Van Zee, A.M. LaPointe, G.W. Coates, Chem. Rev. 114 (2014) 8129–8152.
[12] S. Pulla, C.M. Felton, P. Ramidi, Y. Gartia, N. Ali, U.B. Nasini, A. Ghosh, J. CO_2 Util. 2 (2013) 49–57.
[13] N. Kielland, C.J. Whiteoak, A.W. Kleij, Adv. Synth. Catal. 355 (2013) 2115–2138.
[14] X.-B. Lu, D.J. Darensbourg, Chem. Soc. Rev. 41 (2012) 1462–1484.
[15] Y. Tsuji, F. Fujihara, Chem. Commun. 48 (2012) 9956–9964.
[16] K. Huang, C.-L. Sun, Z.-J. Shi, Chem. Soc. Rev. 40 (2011) 2435–2452.
[17] M. North, R. Pasquale, C. Young, Green Chem. 12 (2010) 1514–1539.
[18] A. Correa, R. Martin, Angew. Chem. Int. Ed. 48 (2009) 6201–6204.
[19] T. Fan, X. Chen, Z. Lin, Chem. Commun. 48 (2012) 10808–10828.
[20] M. Drees, M. Cokoja, F.E. Kühn, ChemCatChem 4 (2012) 1703–1712.
[21] W.Z. Zhang, W.J. Li, X. Zhang, H. Zhou, X.B. Lu, Org. Lett. 12 (2010) 4748–4751.
[22] R. Yuan, Z. Lin, ACS Catal. 4 (2014) 4466–4473.
[23] S. Grimme, J. Comput. Chem. 27 (2006) 1787–1799.
[24] D. Yu, Y. Zhang, Proc. Nat. Acad. Sci. 107 (2010) 20184–20189.
[25] L. Yang, Y. Yuan, H. Wang, N. Zhang, S. Hing, RSC Adv. 4 (2014) 32457–32466.
[26] H.D. Velázquez, Z.-H. Wu, M. Vandichel, F. Verpoort, Catal. Lett. 147 (2017) 463–471.
[27] S. Grimme, J. Antony, S. Ehrlich, H.J. Krieg, Chem. Phys. 132 (2010) 154104.
[28] S.V.C. Vummaleti, G. Talarico, S.P. Nolan, L. Cavallo, A. Poater, Org. Chem. Front 3 (2016) 19–23.
[29] T. Fujihara, K. Nogi, T. Xu, J. Terao, Y. Tsuji, J. Am. Chem. Soc. 134 (2012) 9106–9109.
[30] F.B. Sayyed, Y. Tsuji, S. Sakaki, Chem. Commun. 49 (2013) 10715–10717.
[31] K. Ukai, M. Aoki, J. Takaya, N. Iwasawa, J. Am. Chem. Soc. 128 (2006) 8706–8707.
[32] H. Qin, J. Han, J. Hao, E.B. Kantchev, Green Chem. 16 (2014) 3224–3229.
[33] H. Mizuno, J. Takaya, N. Iwasawa, J. Am. Chem. Soc. 133 (2011) 1251–1253.
[34] X. Lv, L. Zhang, B. Sun, Z. Li, Y.-B. Wu, G. Lu, Catal. Sci. Technol. 7 (2017) 3539–3545.
[35] T. Ohishi, M. Nishiura, Z. Hou, Angew. Chem. Int. Ed. 47 (2008) 5792–5795.
[36] L. Dang, Z. Lin, T.B. Marder, Organometallics 29 (2010) 917–927.
[37] T.G. Ostapowicz, M. Hölscher, W. Leitner, Chem. Eur J. 17 (2011) 10329–10338.
[38] T. León, A. Correa, R. Martin, J. Am. Chem. Soc. 135 (2013) 1221–1224.
[39] F.B. Sayyed, S. Sakaki, Chem. Commun. 50 (2014) 13026–13029.
[40] T. Fujihara, T. Xu, K. Semba, J. Terao, Y. Tsuji, Angew. Chem. Int. Ed. 50 (2011) 523–527.
[41] J.-F. Wang, J.-F. Jia, C.H. Guo, H.S. Wu, J. Organomet. Chem. (2013) 84–88.
[42] T.M. Fan, F.K. Sheong, Z. Line, Organometallics 32 (2013) 5224–5230.
[43] T.G. Ostapowicz, M. Hölscher, W. Leitner, Eur. J. Inorg. Chem. (2012) 5632–5641.
[44] C.M. Williams, J.B. Johnson, T. Rovis, J. Am. Chem. Soc. 130 (2008) 14936–14937.
[45] R. Yuan, Z. Lin, Organometallics 33 (2014) 7147–7156.
[46] Q. Wang, C.H. Guo, Y. Ren, H.-S. Wu, J. Mol. Model. 21 (2015) 122.
[47] J. Takaya, N. Iwasawa, J. Am. Chem. Soc. 130 (2008) 15254–15255.
[48] a) M.T. Johnson, R. Johansson, M.V. Kondrashov, G. Steyl, M.S.G. Ahlquist, A. Roodt, O.F. Wendt, Organometallics 29 (2010) 3521–3529;
b) J. Wu, J.C. Green, N. Hazari, D.P. Hruszkewycz, C.D. Incarvito, T.J. Schmeier, Organometallics 29 (2010) 6369–6376;
c) M. Wang, T. Fan, Z. Lin, Polyhedron 32 (2012) 35–40.
[49] T.W. Butcher, E.J. McClain, T.G. Hamilton, T.M. Perrone, K.M. Kroner,

G.C. Donohoe, N.G. Akhmedov, J.L. Petersen, B.V. Popp, Org. Lett. 18 (2016) 6428–6431.
[50] X. Lv, Y.-B. Wu, G. Lu, Catal. Sci. Technol. 7 (2017) 5049–5054.
[51] G. Herzberg, Electronic Spectra and Electronic Structure of Polyatomic Molecules, Van Nostrand, New York, 1966.
[52] T.J. Schmeier, N. Hazari, C.D. Incarvito, J.A. Raskatov, Chem. Commun. 47 (2011) 1824–1826.
[53] Lj. Pavlovic, J. Vaitla, A. Bayer, K.H. Hopmann, Rhodium-catalyzed hydrocarboxylation: mechanistic analysis reveals unusual transition state for C-C bond formation (submitted for publication).
[54] C. Cramer, D.G. Truhlar, Phys. Chem. Chem. Phys. 11 (2009) 10757–10816.
[55] K.H. Hopmann, Organometallics 35 (2016) 3795–3807.
[56] G. Morello, K.H. Hopmann, ACS Catal. 7 (2017) 5847–5855.

Please cite this article in press as: M. Obst, et al., Journal of Organometallic Chemistry (2018), https://doi.org/10.1016/j.jorganchem.2018.02.020